第 31 卷第 5 期
2015 年 5 月

无 机 化 学 学 报
CHINESE JOURNAL OF INORGANIC CHEMISTRY

Vol.31 No.5
1041-1048

三维 Mn(Ⅱ)-Sm(Ⅲ)杂核和二维同核 Sm(Ⅲ)配合物的合成、晶体结构与性质

陈满生*,[1,2] 邓奕芳[2] 崔 莺[2] 刘冬成[1] 梁福沛*,[1]

([1]广西师范大学化学与药学学院,桂林 541004)

([2]衡阳师范学院化学与材料科学系,功能金属有机材料湖南省普通高等学校重点实验室,衡阳 421008)

摘要: 利用过渡金属锰盐与稀土盐水热合成了杂核化合物{[$MnSm_2(INAIP)_4(H_2O)_4$]·$2H_2O$}$_n$ (**1**)和同核{[Sm(INAIP)(HINAIP)]·$2H_2O$}$_n$ (**2**)(INAIP=异烟酰胺吡啶基异酞酸根),并对其进行了元素分析、IR 及 X-射线衍射法表征。晶体结构研究表明:配合物 **1** 属于三斜晶系,$P\bar{1}$ 空间群。晶胞参数:a=1.018 8(5) nm,b=1.083 86(6) nm,c=1.387 21(8) nm,V=1.475(14) nm^3,Z=1,D_c=1.802 g·cm^{-3},μ=2.271 mm^{-1},F(000)=793,R_{int}=0.010 5,R_1=0.051 2,wR_2=0.131 9。配合物 **2** 属于单斜晶系,$P2_1/c$ 空间群。晶胞参数:a=1.343 05(18) nm,b=1.376 5(17) nm,c=1.62408(15) nm,V=2.7028(6) nm^3,Z=4,D_c=1.861 g·cm^{-3},μ=2.251 mm^{-1},F(000)=1 500,R_{int}=0.051 4,R_1=0.032 2,wR_2=0.088 7。配合物 **1** 是由配体 INAIP 连接稀土钐离子形成二维层状结构,该二维层通过 Mn-O 和 Mn-N 键连接成三维非贯穿网络结构。而配合物 **2** 是由配体 INAIP 连接稀土钐离子形成二维双层状结构,该二维层通过氢键连接成三维网络结构。配合物 **1** 失去水分子后具有稳定微孔结构,对二氧化碳具有一定的吸附,而对氮气没有吸附作用。此外,配合物 **1** 和 **2** 具有典型的稀土钐离子红色荧光性能。

关键词: 杂核配合物; 晶体结构; 5-异烟酰胺吡啶基异酞酸; 水热合成

中图分类号: O614.33+7 **文献标识码**: A **文章编号**: 1001-4861(2015)05-1041-08

DOI: 10.11862/CJIC.2015.130

Syntheses, Crystal Structures and Properties of 3D Heteronuclear Mn(Ⅱ)-Sm(Ⅲ) and 2D Homonuclear Sm(Ⅲ) Complexes

CHEN Man-Sheng*,[1,2] DENG Yi-Fang[2] CUI Ying[2] LIU Dong-Cheng[1] LIANG Fu-Pei*,[1]

([1]*School of Chemistry and Pharmaceutical Sciences, Guangxi Normal University, Guilin, Guangxi* 541004, *China*)

([2]*Department of chemistry and Materials Science, Key Laboratory of Functional Organometallic Materials of Hunan Province College, Hengyang Normal University, Hengyang, Hunan* 421008, *China*)

Abstract: Two heteronuclear/homonuclear coordination polymers {[$MnSm_2(INAIP)_4(H_2O)_4$]·$2H_2O$}$_n$ (**1**) and {[Sm(INAIP)(HINAIP)]·$2H_2O$}$_n$ (**2**), where H_2INAIP=5-(isonicotinamido)isophthalic acid, were synthesized in a pot and their crystal structures were determined by X-ray diffraction analysis. Complex **1** crystallizes in the triclinic system, space group $P\bar{1}$ with a=1.018 8(5) nm, b=1.083 86(6) nm, c=1.387 21(8) nm, V=1.475(14) nm^3, Z=1, D_c=1.802 g·cm^{-3}, μ=2.271 mm^{-1}, F(000)=793, R_{int}=0.010 5, R_1=0.051 2, wR_2=0.131 9. Complex **2** is of monoclinic system, space group $P2_1/c$ with a=1.343 05(18) nm, b=1.376 5(17) nm, c=1.624 08(15) nm, V=2.702 8(6) nm^3, Z=4, D_c=1.861 g·cm^{-3}, μ=2.251 mm^{-1}, F(000)=1 500, R_{int}=0.051 4, R_1=0.032 2, wR_2=0.088 7. In complex **1**, the 2D Sm-carboxylate layer is linked by Mn-N and Mn-O interaction into complicated 3D framework. However, for complex **2**, the central Sm(Ⅲ) atom is eight-coordinated by eight carboxylate oxygen atoms. The molecules are

收稿日期:2014-12-24。收修改稿日期:2015-01-30。

国家自然科学基金(No.21461004,21271050),中国博士后科学基金(No.2014M552534XB),湖南省教育厅重点项目(No.14A021),福建省教育厅 A 类重点(No.JA14261),功能金属有机材料湖南省普通高等学校重点实验室项目(No.13K06)资助和湖南省重点学科建设项目资助。

*通讯联系人。E-mail:cmsniu@163.com,liangfupei@glut.edu.cn;会员登记号:S06N7223M1009。

connected to form a 2D bilayer structure bridged by 5-(isonicotinamido)isophthalic acid. Furthermore, complex **1** shows adsorption behavior of CO_2 with almost no N_2 uptake, and the luminescent property of complexes **1** and **2** has also been investigated. CCDC: 1045729, **1**; 1045730, **2**.

Key words: heteronuclear complex; crystal structure; 5-(isonicotinamido)isophthalic acid; hydrothermal synthesis

0 Introduction

It is well known that the self-assembly of metal-organic frameworks (MOFs) is nowadays considered as one of the most popular fields in coordination and supramolecular chemistry due to their potential applications as functional materials including porosity, magnetism, ion exchange, catalysis and so on[1-7]. Among them, homonuclear coordination polymers have been widely studied. However, heteronuclear complexes containing 3*d*-4*f* metal ions have been less reported. The selection of ligand containing appropriate coordination sites is also crucial to construct exciting frameworks, because the nature of the ligand, the arrangement of the donor atoms and the coordination modes may control the final structures[8-13]. On the other hand, lanthanide ions behave as hard acids and they prefer O-donors to N-donors, while *d*-block metal ions are borderline acids, having a strong tendency to coordinate to both N-donors and O-donors. Considering the fact that N and O atoms have different affinities to transition-metal and lanthanide ions, respectively, a typical approach toward the construction of *d*-*f* heterometallic frameworks can be the reaction of a mixture of *d*-*f* metal ions with a single multidentate bridging ligand containing both N- and O-donor atoms. Furthermore, 5-(isonicotinamido) isophthalic acid as a bifunctional bridging ligand possesses oxygen and nitrogen donors, which can be chosen to as a potential linker between the lanthanide centers and the transition metal centers[14-15]. On the basis of the above-mentioned considerations, in this paper, we have synthesized a 3*d*-4*f* and a 4*f* coordination polymers through hydrothermal reaction in a pot, namely $[MnSm_2(INAIP)_4(H_2O)_4]\cdot 2H_2O$ (**1**) and [Sm(INAIP)(HINAIP)]·$2H_2O$ (**2**) (H_2INAIP=5-(isonicotinamido)isophthalic acid). The gas adsorption and photoluminescence were investigated.

1 Experimental

1.1 Materials and instruments

The regents were used as commercial sources without further purification. Elemental analyses were performed on a Perkin-Elmer 240C elemental analyzer. The IR spectra were recorded on Bruker Vector22 FT-IR spectrophotometer using KBr discs. Thermogravimetric analyses were performed on a simultaneous SDT 2960 thermal analyzer under nitrogen with a heating rate of 10 ℃·min^{-1}. Powder X-ray diffraction (PXRD) patterns were measured on a Shimadzu XRD-6000 X-ray diffractometer with Cu $K\alpha$ (λ=0.154 18 nm) radiation at room temperature. The luminescent spectra for the solid powdered samples were recorded at room temperature on an Aminco Bowman Series 2 spectrophotometer with xenon arc lamp as the light source. In the measurements of the emission and excitation spectra, the pass width was 4.0 nm. All the measurements were carried out under the same conditions. Gas sorption isotherms were measured on a volumetric adsorption apparatus (Bel-max).

1.2 Synthesis of the complexes 1 and 2

Complexes **1** and **2** were synthesized by hydrothermal method in a 16 mL Teflon-lined autoclave by heating a mixture of $Sm(NO_3)_3\cdot 6H_2O$ (0.05 mmol, 22.5 mg), $MnCl_2$ (0.05 mmol, 7.2 mg), H_2INAIP (0.1 mmol, 28.7 mg), NaOH (0.15 mmol, 6.0 mg) and H_2O (10 mL) at 150 ℃ for 3 d under autogenous pressure. Cooling the reactor subsequently to room temperature at a rate of 10 ℃·h^{-1}, pale-yellow crystals of **1** and colorless **2** were obtained, and their crystals were manually separated from the resulting powder samples under a microscope. For **1**, IR(cm^{-1}): 3 423(s), 2 936 (w), 1 659(m), 1 548(s), 1 526(s), 1 445(s), 1 380(s), 1 237(m), 1 109(m), 886(s), 783(s), 602(w). Anal.

Calcd. For $C_{56}H_{44}MnSm_2N_8O_{26}$ (%): C 41.98, H 2.75, N 7.00; Found (%): C 41.93, H 2.78, N 6.95. For **2**, IR (cm^{-1}): 3 398(s), 1 674(s), 1 605(m), 1 559(m), 1 525 (m), 1 497(w), 1 426(m), 1 383(s), 1 324(m), 1 068 (m), 790 (m), 674 (w), 594 (w) Anal. Calcd. For $C_{28}H_{21}SmN_4O_{12}$ (%): C 44.45, H 2.78, N 7.41; Found (%): C 44.49, H 2.75, N 7.35.

1.3 X-ray crystallography

The crystals with dimensions of 0.27 mm×0.23 mm×0.21 mm and 0.20 mm×0.15 mm×0.12 mm were selected for the measurement. The diffraction data were collected on a Bruker Smart Apex Ⅱ CCD diffractometer equipped with a graphite-monochromatized Mo $K\alpha$ radiation (λ=0.071 073 nm). The data were integrated by using the SAINT program[16], which also did the intensity corrections for Lorentz and polarization effect. An empirical absorption correction was applied using the SADABS program[17]. The structures were solved by direct methods using the program SHELXS-97 and all the non-hydrogen atoms were refined anisotropically on F^2 by the full-matrix least-squares technique using the SHELXL-97 crystallographic software package[18-19]. Crystal data and structure refinement parameters are listed in Table 1. The selected bond lengths and bond angles are given in Table 2.

CCDC: 1045729, **1**; 1045730, **2**.

Table 1　Crystal data and structure parameters for the title complexes

Complex	**1**	**2**
Empirical formula	$C_{56}H_{44}MnSm_2N_8O_{26}$	$C_{28}H_{21}SmN_4O_{12}$
Formula weight	1 600.63	755.85
Crystal system	Triclinic	Monoclinic
Space group	$P\bar{1}$	$P2_1/c$
a / nm	1.018 8(5)	1.343 05(18)
b / nm	1.083 86(6)	1.376 50(17)
c / nm	1.387 21(8)	1.624 08(15)
V / nm^3	1.475 0(14)	2.702 8(6)
Z	1	4
Absorption coefficient / mm^{-1}	2.271	2.251
F(000)	793	1500
Reflections collected / unique	8 055 / 5 663 (R_{int}=0.010 5)	13 754 / 5 011 (R_{int}=0.051 4)
Data / restraints / parameters	5 663 / 0 / 423	5 011 / 0 / 406
Final R indices ($I>2\sigma(I)$)	R_1=0.051 2, wR_2=0.131 9	R_1=0.032 2, wR_2=0.088 7
Largest diff. peak and hole / ($e\cdot nm^{-3}$)	952 and −765	1 213 and −669

Table 2　Selected bond lengths (nm) and bond angles (°) for complexes 1 and 2

1					
Mn(1)-O(2W)	0.222 9(4)	Mn(1)-N(2C)	0.2271(5)	Mn(1)-O(7)	0.216 5(4)
Sm(1)-O(1)	0.249 7(4)	Sm(1)-O(3A)	0.252 3(4)	Sm(1)-O(2)	0.241 3(4)
Sm(1)-O(4A)	0.242 8(4)	Sm(1)-O(6)	0.224 8(4)	Sm(1)-O(8B)	0.244 0(4)
Sm(1)-O(1W)	0.238 5(4)	Sm(1)-O(9B)	0.242 8(4)		
O(7)-Mn(1)-O(2W)	85.88(17)	O(7)-Mn(1)-N(2C)	88.14(16)	O(2W)-Mn(1)-N(2C)	89.45(17)
O(6)-Sm(1)-O(1W)	82.75(14)	O(6)-Sm(1)-O(2)	89.94(13)	O(1W)-Sm(1)-O(2)	138.34(14)
O(6)-Sm(1)-O(9B)	153.96(13)	O(1W)-Sm(1)-O(9B)	121.24(14)	O(2)-Sm(1)-O(9B)	78.39(14)
O(6)-Sm(1)-O(4A)	81.87(13)	O(1W)-Sm(1)-O(4A)	139.42(14)	O(2)-Sm(1)-O(4A)	78.90(13)
O(9B)-Sm(1)-O(4A)	73.13(13)	O(6)-Sm(1)-O(8B)	153.05(13)	O(1W)-Sm(1)-O(8B)	70.99(13)
O(2)-Sm(1)-O(8B)	105.49(14)	O(9B)-Sm(1)-O(8B)	52.83(12)	O(4A)-Sm(1)-O(8B)	122.24(13)

Continued Table 2

O(6)-Sm(1)-O(1)	85.60(14)	O(1W)-Sm(1)-O(1)	85.76(14)	O(2)-Sm(1)-O(1)	52.27(13)
O(9B)-Sm(1)-O(1)	104.79(14)	O(4A)-Sm(1)-O(1)	129.92(13)	O(8B)-Sm(1)-O(1)	86.45(14)
O(6)-Sm(1)-O(3A)	84.41(14)	O(1W)-Sm(1)-O(3A)	88.16(13)	O(2)-Sm(1)-O(3A)	132.02(13)
O(9B)-Sm(1)-O(3A)	86.32(14)	O(4A)-Sm(1)-O(3A)	53.12(13)	O(8B)-Sm(1)-O(3A)	100.29(14)
O(1)-Sm(1)-O(3A)	168.89(15)				
			2		
Sm(1)-O(6)	0.236 6(3)	Sm(1)-O(4B)	0.245 4(3)	Sm(1)-O(3A)	0.236 9(3)
Sm(1)-O(2)	0.265 2(3)	Sm(1)-O(7C)	0.238 2(3)	Sm(1)-O(8D)	0.250 7(3)
Sm(1)-O(1)	0.243 5(3)	Sm(1)-O(9D)	0.249 1(3)		
O(6)-Sm(1)-O(3A)	73.68(9)	O(6)-Sm(1)-O(7C)	126.32(9)	O(3A)-Sm(1)-O(7C)	79.04(9)
O(6)-Sm(1)-O(1)	79.67(10)	O(3A)-Sm(1)-O(1)	146.63(10)	O(7C)-Sm(1)-O(1)	133.87(9)
O(6)-Sm(1)-O(4B)	83.26(9)	O(3A)-Sm(1)-O(4B)	123.91(10)	O(7C)-Sm(1)-O(4B)	74.99(9)
O(1)-Sm(1)-O(4B)	71.15(9)	O(6)-Sm(1)-O(9D)	153.47(9)	O(3A)-Sm(1)-O(9D)	126.92(9)
O(7C)-Sm(1)-O(9D)	77.90(9)	O(1)-Sm(1)-O(9D)	74.70(9)	O(4B)-Sm(1)-O(9D)	94.74(9)
O(6)-Sm(1)-O(8D)	133.14(9)	O(3A)-Sm(1)-O(8D)	78.10(9)	O(7C)-Sm(1)-O(8D)	82.53(9)
O(1)-Sm(1)-O(8D)	107.50(9)	O(4B)-Sm(1)-O(8D)	143.46(9)	O(9D)-Sm(1)-O(8D)	51.98(8)
O(6)-Sm(1)-O(2)	76.52(9)	O(3A)-Sm(1)-O(2)	102.66(9)	O(7C)-Sm(1)-O(2)	155.57(9)
O(1)-Sm(1)-O(2)	50.83(8)	O(4B)-Sm(1)-O(2)	120.77(9)	O(9D)-Sm(1)-O(2)	82.01(8)
O(8D)-Sm(1)-O(2)	74.15(10)				

Symmetry code for **1**: A: −1+*x*, *y*, *z*, B: *x*, 1+*y*, *z*, C: 1−*x*, 1−*y*, −*z*; For **2**: A: 2−*x*, −1/2+*y*, 3/2−*z*, B: *x*, 1/2−*y*, −1/2+*z*, C: 2−*x*, −*y*, 1−*z*, D: 2−*x*, −1/2+*y*, 3/2−*z*.

2 Results and discussion

2.1 Crystal structure of the title complexes

The single-crystal X-ray diffraction analysis revealed that complex **1** crystallized in the triclinic system with space group $P\bar{1}$. As illustrated in Fig.1a, the asymmetric unit of **1** consists of one Sm(Ⅲ) atom, half Mn(Ⅱ) atom, two $INAIP^{2-}$ ligands, two coordinated and one lattice water molecules. Each Mn(Ⅱ) cation is located on an inversion center and is coordinated by two pyridine N atoms, two carboxylate O atoms and two water molecules in a slightly distorted octahedral geometry. On the other hand, each Sm(Ⅲ) ion is eight-coordinated by seven carboxylate oxygen atoms from four different $INAIP^{2-}$ ligands and one from a coordinated water molecule. The Sm center can be described as having a distorted square antiprismatic coordination geometry with Sm-O bond distances ranging from 0.224 8(4) to 0.252 3(4) nm, which is in agreement to those observed in other Ln-INAIP complexes. In the structure of **1**, it is note that the two $INAIP^{2-}$ ligands have two different kinds of coordination modes: One coordinated to two Sm(Ⅲ) and one Mn(Ⅱ) atoms using its two carboxylate groups with chelate and bridging coordination modes while the pyridyl group is free of coordination; the other one coordinated to two Sm(Ⅲ) through the carboxylate groups only with chelate coordination mode and the pyridyl group connected one Mn(Ⅱ) atom. Finally, the non-interpenetrated 3D framework is formed by these coordination interactions (Fig.1c).

To gain a better visualization and understand the structure of **1**, topological analysis by reducing multidimensional structure to simple node-and-linker net was performed. Based on the simplification principle, each $INAIP^{2-}$ ligand links three metal atoms and can be regarded as a three-connector, and each Sm(Ⅲ) and Mn(Ⅱ) center link four $INAIP^{2-}$ ligands, respectively, which can be regarded as a four-connecting node. Therefore, the final topology of **1**, calculated by TOPOS[20], is a 3,3,4-c net with stoichiometry (3-c)4 (4-c)(4-c)2, 3-nodal net Point (Schläfli)

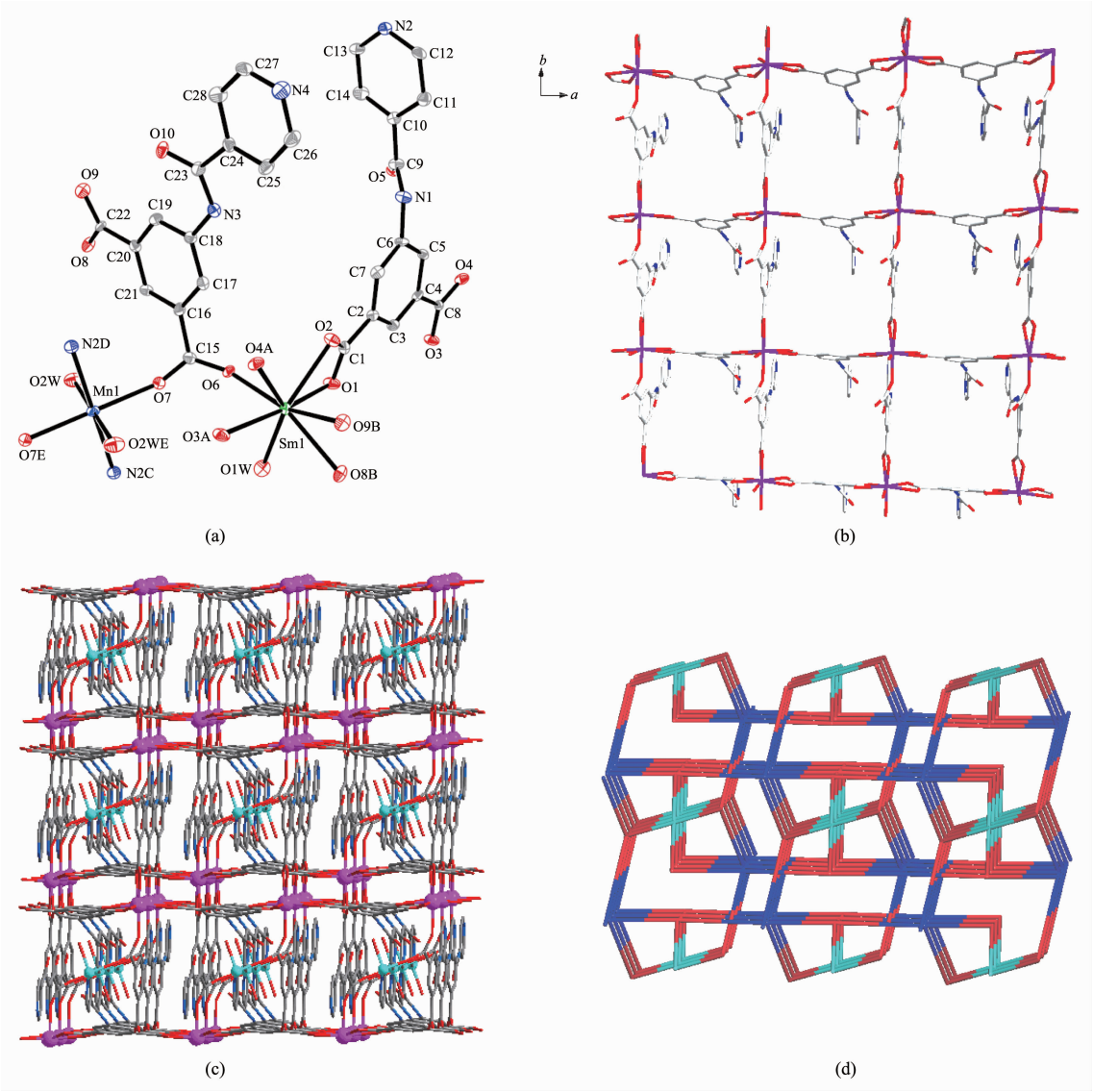

Symmetry code: A: −1+*x*, *y*, *z*; B: *x*, 1+*y*, *z*; C: 1−*x*, 1−*y*, −*z*; D: −1+*x*, *y*, 1+*z*; E: −*x*, 1−*y*, 1−*z*

Fig.1　(a) ORTEP drawing of **1** with 30% thermal ellipsoids (Lattice water molecule and hydrogen atoms are omitted for clarity); (b) 2D network constructed by Sm(Ⅲ) and $INAIP^{2-}$ ligands omitting the pyridyl groups for clarity; (c) View of the 3D framework of **1**; (d) Topological representation of the 3D structure of **1**

symbol for net: $(8^3)_4(8^4\cdot10^2)(8^6)_2$, as shown in Fig.1d.

As illustrated in Fig.2a, the structure of **2** contains of one Sm(Ⅲ) atom, one $INAIP^{2-}$ and one $HINAIP^-$ anion. It is note that full deprotonation of the carboxylate groups of the H_2INAIP ligands in complex **2** was confirmed by IR spectral data, since no strong bands nearby 1 700 cm^{-1} were observed in the IR spectra. However, the charge would unbalance in the resulted complex **2**, therefore the pyridyl groups of one $INAIP^{2-}$ ligand is considered to be protonated and the formula of the complex is written as $\{[Sm(INAIP^{2-})(HINAIP^-)]\cdot2H_2O\}_n$. The Sm(Ⅲ) atom is eight-coordinated and exhibits a distorted square antiprismatic geometry in **2**. It is interesting that the carboxyl groups of two unique $INAIP^{2-}$($HINAIP^-$) ligands exhibit the same coordination modes: one carboxylate group coordinates to one Sm(Ⅲ) atoms in bidentate chelate mode; the other one coordinates to two Sm(Ⅲ) atoms in the same monodentate bridging mode, whereas all the pyridyl groups are free of coordination. Based on the coordination modes of the carboxylate groups of $INAIP^{2-}$ ($HINAIP^-$), a 2D bilayer

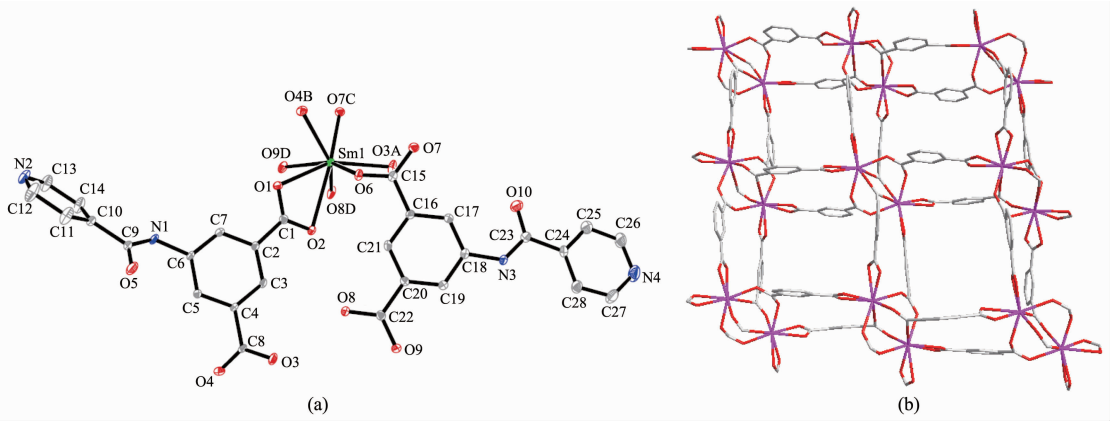

Symmetry code: A: 2–x, –1/2+y, 3/2–z; B: x, 1/2–y, –1/2+z; C: 2–x, –y, 1–z; D: 2–x, –1/2+y, 3/2–z

Fig.2 (a) ORTEP drawing of **2** with 30% thermal ellipsoids (Lattice water molecule and hydrogen atoms are omitted for clarity); (b) 2D bi-layer network constructed by Sm(Ⅲ) and $INAIP^{2-}$ ligands omitting the pyridyl groups for clarity

network is formed (Fig.2b).

Finally, the 2D bilayers packed together through N–H···O and O–H···O hydrogen bonding interactions to generate 3D framework, and those hydrogen bonds also exist in the crystal packing diagram, which further consolidate the structure.

2.2 Thermal analyses, X-ray powder diffraction, gas sorption and photoluminescent properties

The result of thermogravimetric(TG) analyses indicate that complex **1** lost its coordinated and noncoordinated water molecules in the 30 ~170 ℃ temperature range. The weight loss found of 6.69% is consistent with that calculated (6.75%). After the loss of all the H_2O molecules, the 3D framework was stable up to 475 ℃, followed by another weight loss after that temperature. PXRD was used to check the purity of complex **1**. The results show that all the peaks displayed in the measured patterns at room temperature closely match those in the simulated patterns generated from single-crystal diffraction data, indicating single phases of **1** were formed, as shown in Fig.3a.

After omitting all the water molecules, PLATON[21] analysis revealed that the porous structure was composed of large voids of 19.92 nm that represent 13.5% per unit cell volume in **1**. Gas adsorption-desorption isotherms (N_2 and CO_2) for desolvated **1** are shown in Fig.3b. Before gas adsorption tests, the activation for removing the guest molecules and coordinated water molecules from the pores by heating under a vacuum is a required pretreatment and the as-synthesized crystal samples were heated at an optimized temperature of 160 ℃ for 10 hours. The results indicate that almost no N_2 uptake was observed

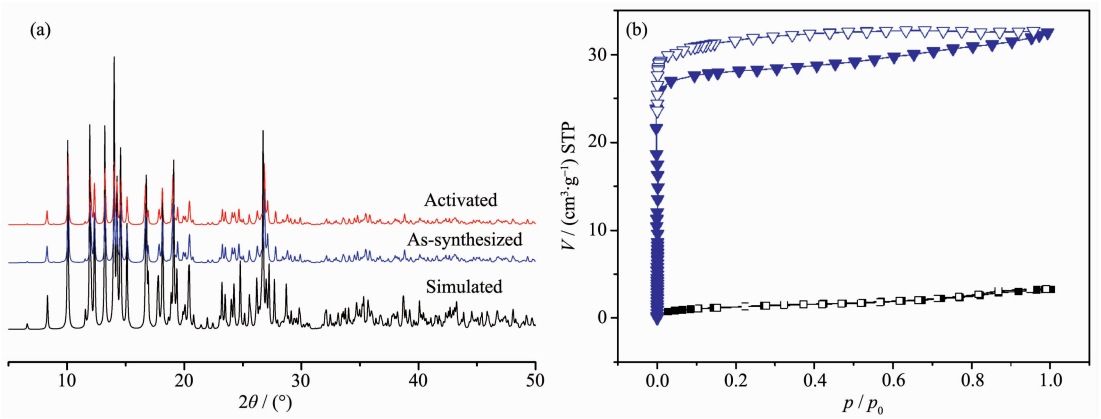

Fig.3 (a) Powder X-ray diffraction patterns of complex **1**; (b) N_2 and CO_2 adsorption isotherm (273 K) of **1** (square and triangle curves represent N_2 and CO_2 adsorption; filled shapes: adsorption; open ones: desorption respectively)

at 273 K, and the hysteresis behavior in which are characteristic for type-H3. It was found that significant amounts of CO_2 (273 K) were adsorbed and the isotherm presented typical type-I curves[22], which is the characteristic of a microporous material. The amounts of CO_2 uptake increase abruptly at the beginning and reach to 32.50 $cm^3 \cdot g^{-1}$(STP) at 100 kPa for **1**. Thus, approximately 0.32 CO_2 molecules per formula unit were adsorbed for **1**. It can be clearly seen from Fig.3b that the gas sorption isotherms show obvious hysteresis between the adsorption-desorption curves. It is note that the selective sorption of CO_2 rather than N_2 gas can also be attributed to the significant quadrupole moment of CO_2 (-1.4×10^{-39} C·m^2), which induces specific interactions with the host framework to open up the channels.

On the other hand, complexes **1** and **2** emit strong red fluorescence under ultraviolet light at room temperature, therefore, the solid-state visible luminescent property of them was investigated. Complex **1** displays red luminescence (Fig.4a) upon excitation at 362 nm, the emissions at 564, 597, and 650 nm are attributed to the characteristic emissions of $^4G_{5/2}\rightarrow{}^6H_{5/2}$, $^4G_{5/2}\rightarrow{}^6H_{7/2}$ and $^4G_{5/2}\rightarrow{}^6H_{9/2}$ transitions of the Sm(Ⅲ) ion. Complex **2** shows red luminescence (Fig.4b) upon excitation at 360 nm, the emissions at 561, 592 and 643 nm can be assigned to the characteristic emissions of $^4G_{5/2}/{}^6H_J$ (J=5/2, 7/2, and 9/2) transitions of the Sm(Ⅲ) ion. The emissions are dominated by the$^4G_{5/2}\rightarrow{}^6H_{7/2}$ transition, peaking at 597, 592 and 604 nm, corresponding to crystal field splitting, which gave a strong red luminescence output for **1** and **2**.

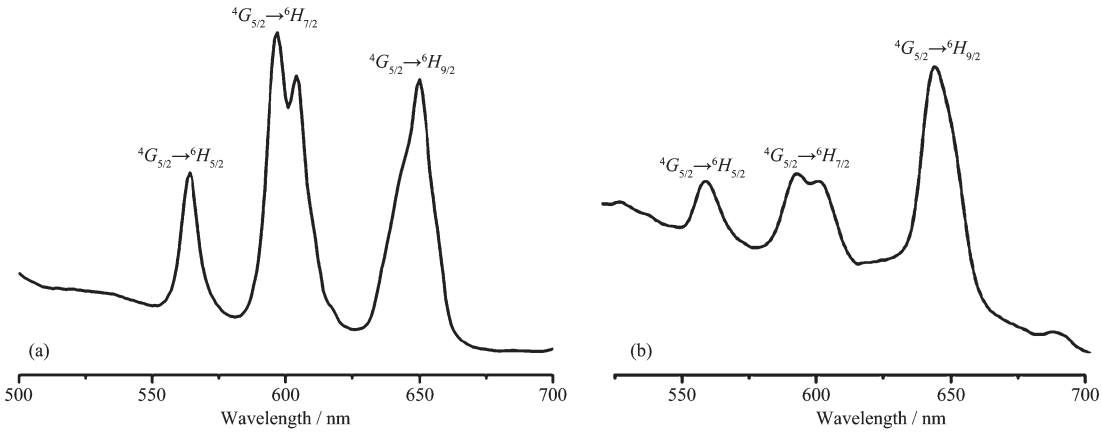

Fig.4　Photoluminescence spectra of complexes **1** (a) and **2** (b) in the solid state at room temperature

References:

[1] Batten S R, Robson R. *Angew. Chem., Int. Ed.*, **1998**,**37**: 1460-1494

[2] Yaghi O M, Li H, Davis C, et al. *Acc. Chem. Res.*, **1998**,**31**: 474-484

[3] Hagrman P J, Hagrman D, Zubieta J. *Angew. Chem., Int. Ed.*, **1999**,**38**:2639-2684

[4] Cote A P, Benin A I, Ockwig N W, et al. *Science*, **2005**,**310**: 1166-1170

[5] Yaghi O M, O′Keeffe M, Ockwig N W, et al. *Nature*, **2003**, **423**:705-714

[6] Wu C D, Hu A, Zhang L, et al. *J. Am. Chem. Soc.*, **2005**, **127**:8940-8941

[7] Kitagawa S, Kitaura R, Noro S. *Angew. Chem. Int. Ed.*, **2004**,**43**:2334-2375

[8] Rosi N L, Kim J, Eddaoudi M, et al. *J. Am. Chem. Soc.*, **2005**,**127**:1504-1518

[9] Su Z, Fan J, Chen M, et al. *Cryst. Growth Des.*, **2011**,**11**: 1159-1169

[10]Zhang Y B, Zhang W X, Feng F Y, et al. *Angew. Chem., Int. Ed.*, **2009**,**48**:5287-5290

[11]Park J, Yuan D Q, Pham K T, et al. *J. Am. Chem. Soc.*, **2012**,**134**:99-102

[12]Gotthardt J M, White K F, Abrahams B F, et al. *Cryst. Growth Des.*, **2012**,**12**:4425-4430

[13]James S L. *Chem. Soc. Rev.*, **2003**,**32**:276-288

[14]Chen M S, Su Z, Chen M, et al. *CrystEngComm*, **2010**,**12**: 3267-3276

[15]CHEN Man-Sheng(陈满生), LUO Li(罗莉), CHEN Shui-Sheng(陈水生), et al. *Chinese J. Inorg. Chem.*(无机化学学报), **2010**,**26**:2227-2232

[16]*SAINT, Version* 6.02*a*. Bruker AXS Inc., Madison, W1, **2002**.

[17]Sheldrick G M. *SADABS, Program for Bruker Area Detector Absorption Correction*, University of Göttingen, Göttingen, Germany, **1997**.

[18]Sheldrick G M. *SHELXS*-97, *Program for Crystal Structure Solution*, University of Göttingen, Göttingen, Germany, **1997**.

[19]Sheldrick G M. *SHELXL*-97, *Program for Crystal Structure Refinement*, University of Göttingen, Göttingen, Germany, **1997**.

[20]Blatov V A. *IUCr CompComm Newsletter*, **2006**,**7**:4-38

[21]Spek A L. *J. Appl. Crystallogr.*, **2003**,**36**:7-13

[22]Zhong D C, Lin J B, Lu W G, et al. *Inorg. Chem.*, **2009**,**48**: 8656-8658